Leon S. Dimas
Laboratory for Atomistic and Molecular Mechanics (LAMM),
Department of Civil and Environmental Engineering,
Massachusetts Institute of Technology,
77 Massachusetts Avenue,
Cambridge, MA 02139;
Department of Civil and Environmental Engineering,
Massachusetts Institute of Technology,
77 Massachusetts Avenue,
Cambridge, MA 02139

Daniele Veneziano
Department of Civil and Environmental Engineering,
Massachusetts Institute of Technology,
77 Massachusetts Avenue,
Cambridge, MA 01239

Tristan Giesa
Laboratory for Atomistic and Molecular Mechanics (LAMM),
Department of Civil and Environmental Engineering,
Massachusetts Institute of Technology,
77 Massachusetts Avenue,
Cambridge, MA 02139;
Department of Civil and Environmental Engineering,
Massachusetts Institute of Technology,
77 Massachusetts Avenue,
Cambridge, MA 02139

Markus J. Buehler[1]
Laboratory for Atomistic and Molecular Mechanics (LAMM),
Department of Civil and Environmental Engineering,
Massachusetts Institute of Technology,
77 Massachusetts Avenue,
Cambridge, MA 02139;
Department of Civil and Environmental Engineering,
Massachusetts Institute of Technology,
77 Massachusetts Avenue,
Cambridge, MA 02139
e-mail: mbuehler@MIT.EDU

Random Bulk Properties of Heterogeneous Rectangular Blocks With Lognormal Young's Modulus: Effective Moduli

We investigate the effective elastic properties of disordered heterogeneous materials whose Young's modulus varies spatially as a lognormal random field. For one-, two-, and three-dimensional (1D, 2D, and 3D) rectangular blocks, we decompose the spatial fluctuations of the Young's log-modulus $F = \ln E$ into first- and higher-order terms and find the joint distribution of the effective elastic tensor by multiplicatively combining the term-specific effects. The analytical results are in good agreement with Monte Carlo simulations. Through parametric analysis of the analytical solutions, we gain insight into the effective elastic properties of this class of heterogeneous materials. The results have applications to structural/mechanical reliability assessment and design.
[DOI: 10.1115/1.4028783]

1 Introduction

Elastic homogenization is the problem of determining the bulk or effective moduli of heterogeneous elastic bodies from the geometric arrangement and properties of the component phases. The literature on elastic homogenization is vast; see, for example, Refs. [1–5] for book reviews spanning several decades. The typical setup, which is appropriate for many natural and manufactured materials, considers a homogeneous matrix in which inclusions made of one or several other phases are present. A less studied case is when the local elastic properties of a single material vary spatially in a random but continuous manner, for example due to spatial variations in material density (as in bone) or in the arrangement and properties of unresolved microconstituents (as in cement, soils and other geologic materials). Of course, one may combine the two sources of variability by considering multiphase composites in which the elastic properties vary not only from phase to phase, but also spatially within each phase.

Here, we address the homogenization problem for single-phase rectangular blocks of Euclidean dimension $n = 1$, 2, or 3, in which the elastic Young's modulus E varies spatially as an isotropic lognormal field. Recent experimental studies indicate that various materials exhibit similar local variations in mechanical properties [6–9]. Several of these, and related, investigations suggest that the local variation in mechanical properties lead to enhanced bulk

[1]Corresponding author.

Contributed by the Applied Mechanics Division of ASME for publication in the Journal of Applied Mechanics. Manuscript received September 21, 2014; final manuscript received October 9, 2014; accepted manuscript posted October 13, 2014; published online November 14, 2014. Editor: Yonggang Huang.

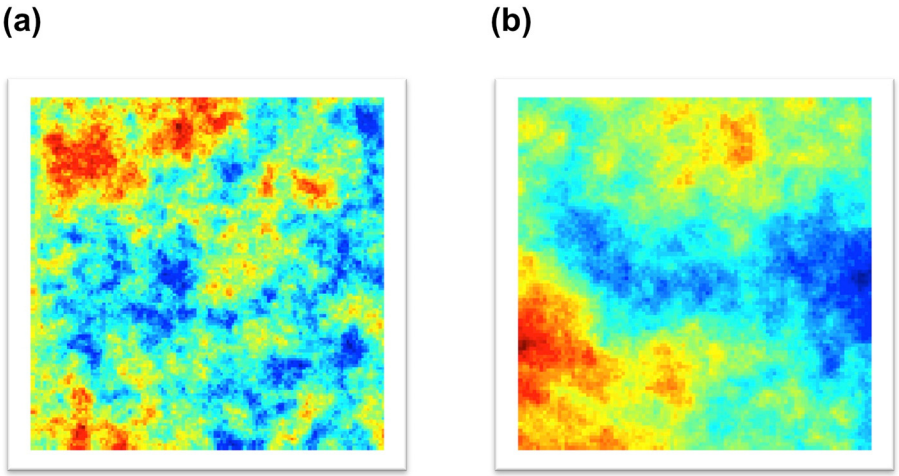

Fig. 1 Realizations of 2D normal log-stiffness fields with a simple exponential correlation kernel for normalized correlation lengths of (*a*) 0.125 and (*b*) 0.5

mechanical properties [7,8,10]. There is thus a significant interest in developing a fundamental understanding of the bulk properties of materials with such local heterogeneities. In Fig. 1, we present two realizations of 2D normal log-stiffness fields. The fields are simulated with a simple exponential correlation function with normalized correlation lengths of 0.125 and 0.5 for (a) and (b), respectively. When the size of the block is very large compared with the characteristic scale of the heterogeneities (a case we refer to as the ergodic limit), the effective properties become deterministic [11]. In the literature a block at this length scale is commonly referred to as a representative volume element [12]. However, for blocks of finite size, which is the case considered here, the effective properties are stochastic and must be characterized through joint probability distributions.

Numerically, this problem is typically addressed through various stochastic finite element methods [13–18]. These studies focus on the numerical analysis of the problem, with spectral and Monte Carlo methods among the notable techniques to derive distributions of quantities of interest through numerical simulation. Other numerical approaches have focused on spring-network discretizations of the random microstructures [19,20]. There is also significant interest in analytical solutions to the problem [21–25]. A particularly interesting technique is the use of variability response functions (VRFs), first introduced by Shinozuka [25]. VRFs can be used to find the analytical solutions to response variability of statically determinate beam structures [21,25]. To analyze more general problems, generalized variability response functions (GVRFs) have been developed. These require the use of a limited number of Monte Carlo simulations and can describe the response variability of statically indeterminate beam structures and certain 2D systems [26,27]. To the best of the authors' knowledge no studies have investigated the usefulness of GVRFs for the variable response prediction of 3D systems.

In this study we use a full analytical approach and develop analytical expressions for the joint distributions of the effective elastic tensor. Our approach is to make an analysis-of-variance (ANOVA) decomposition of the Young's log-modulus field $F(x) = \ln E(x)$ as the sum of the average value inside the block, the marginal fluctuations along the coordinate axes ("main effects"), and interactions of order $2, \ldots, n$. Then, we evaluate the effect of each ANOVA term on the effective moduli in tension $E_{\text{eff},i}$ and shear $G_{\text{eff},ij}$. The desired distribution of the bulk moduli is the product of these term-specific effects. The term effects are obtained exactly or with high accuracy for the low-order ANOVA components and under simplifying approximations for the higher-order interactions. The most drastic approximation is that the higher-order effects are deterministic and can be estimated from the ergodic results. Since the higher-order terms make relative small contributions to the effective moduli, the resulting approximations are accurate. A similar ANOVA approach was used by Veneziano and Tabaei [28] to approximate the distribution of the effective hydraulic conductivity of heterogeneous porous blocks. Here, we adapt that methodology to the elastic problem.

After validation through Monte Carlo simulation, we use the ANOVA results to analyze how the distribution of the effective moduli varies with the Euclidean dimension n, the size and shape of the block, and the variance and correlation of the $F(x)$ field. In addition to contributing to the fundamental understanding of the mechanics of disordered materials, these results can be used to assess and control the reliability of structures made of random composite materials.

2 Probabilistic Model and ANOVA Decomposition

We consider a rectangular n-dimensional block Ω with side lengths $L_1, \ldots, L_n$, made of linear elastic material. We assume that Poisson's ratio ν is a deterministic constant, while Young's modulus varies spatially as an isotropic lognormal field $E(x)$. Hence, the log-modulus $F(x) = \ln E(x)$ is isotropic normal. These fields are specified through the mean modulus m_{E}, the variance of the log-modulus σ_{F}^2, and the isotropic correlation function of the log-modulus $\rho_{\text{F}}(r)$. Interest is in the distribution of the full elastic tensor C_{ijkl}, which includes the normalized effective Young's moduli $E'_{\text{eff},i} = E_{\text{eff},i}/m_{\text{E}}$ and the shear moduli $G'_{\text{eff},ij} = G_{\text{eff},ij}/m_{\text{G}}$ where $m_{\text{G}} = 1/2(1+\nu)m_{\text{E}}$. Since $E'_{\text{eff},i}$ and $G'_{\text{eff},ij}$ do not depend on m_{E} and m_{G}, in what follows we consider the distributions of $E_{\text{eff},i}$ and $G_{\text{eff},ij}$ under $m_{\text{E}} = m_{\text{G}} = 1$.

Under certain conditions ($\lim_{r\to\infty} \rho_{\text{F}}(r) = 0$ and $L_i \to \infty$), the effective moduli $E_{\text{eff},i}$ and $G_{\text{eff},ij}$ become deterministic functions of the variance σ_{F}^2 and the Euclidean dimension n and are independent of $\rho_{\text{F}}(r)$. We refer to these conditions as the ergodic limit. Using an incremental perturbation approach in which fluctuations of F in progressively higher frequency ranges $\omega < |\underline{\omega}| < \omega + \Delta\omega$ are added, Veneziano [11] found that under these ergodic conditions and for $m_{\text{E}} = 1$

$$E_{\text{eff}} = \begin{cases} e^{-\sigma_{\text{F}}^2}, & n = 1 \\ e^{-\frac{5}{8}\sigma_{\text{F}}^2}, & n = 2 \\ e^{-\frac{7}{15}\sigma_{\text{F}}^2}, & n = 3 \end{cases} \tag{1}$$

The corresponding ergodic value of the shear modulus is $G_{\text{eff}} = c \cdot E_{\text{eff}}$, with E_{eff} in Eq. (1) and $c = 1/2(1+\nu)$.

To study the effective Young's moduli, we subject the rectangular blocks to tension and shear. In the tension experiments we displace one block face uniformly in the direction of its normal, while fixing to zero, the corresponding displacements on the opposite face and the tractions on the rest of the boundary. In the shearing experiments, say on the (x_1, x_2)-plane, we simplify the analytical treatment by modulating the applied shear such that cross sections at different x_3 locations undergo the same average shear deformation. This is accomplished by scaling the applied shear force by the average modulus at location x_3; see details in the supplementary material [29]. On each given (x_1, x_2)-plane, the shear forces are applied uniformly along the boundary.

The ANOVA decomposition of the log-modulus $F(x)$ inside rectangular blocks of different Euclidean dimension n is as follows:

$n = 1$

$$F(x_1) = \bar{F}_1 + \varepsilon_1(x_1) \tag{2}$$

where $\bar{F}_1$ is the average of F along the rod and $\varepsilon_1(x_1) = F(x_1) - \bar{F}_1$is the fluctuation around that average value. $\bar{F}_1$ has mean value $-1/2\sigma_F^2$ and ε_1 averages to zero along the length of the rod.

$n = 2$

$$F(x_1, x_2) = \bar{F}_{12} + \varepsilon_1(x_1) + \varepsilon_2(x_2) + \varepsilon_{12}(x_1, x_2). \tag{3}$$

In analogy with the 1D case, the block average $\bar{F}_{12}$ has mean value $m_F = (-1/2)\sigma_F^2$ and all three ε terms have zero mean (actually, they average to zero along each coordinate direction). When (x_1, x_2) in Eq. (3) is considered random with uniform distribution inside the block Ω, the four components on the right hand side of Eq. (3) are independent normal.

$n = 3$

$$\begin{aligned} F(x_1, x_2, x_3) = \bar{F}_{123} &+ \varepsilon_1(x_1) + \varepsilon_2(x_2) + \varepsilon_3(x_3) + \varepsilon_{12}(x_1, x_2) \\ &+ \varepsilon_{13}(x_1, x_3) + \varepsilon_{23}(x_2, x_3) + \varepsilon_{123}(x_1, x_2, x_3) \end{aligned} \tag{4}$$

Again, the block average $\bar{F}_{123}$ has mean value $m_F = (-1/2)\sigma_F^2$ and the ε terms average to zero along the coordinate directions. When (x_1, x_2, x_3) is considered random with uniform distribution in Ω, the eight components on the right hand side of Eq. (4) are independent normal.

For each decomposition, Table 1 gives expressions for the individual components and their variances.

3 Distribution of the Bulk Moduli

This section summarizes our analytical results on the distribution of the effective elastic moduli. In all cases, the log-moduli $\ln E_{\text{eff},i}$ and $\ln G_{\text{eff},ij}$ are approximated as having joint normal distribution with mean values, variances and correlations given below and in supplementary material: Part A. The derivations (supplementary material: Part A) make simplifying approximations: in some cases a distribution is assumed to be lognormal when its exact form is "between normal and lognormal" and the variance contributions from ANOVA terms of order ≥ 2 are always neglected. The accuracy of the results is assessed in Sec. 4 using Monte Carlo simulation.

Results for the mean values μ and variances σ^2 of the log-moduli are summarized below. Expressions for the correlation coefficients in 2D and 3D are given in supplementary material: Part A.

3.1 n = 1 (1D Bar of Length L_1). In the 1D case, E_{eff} is the harmonic average of $E(x)$ along the rod and $G_{\text{eff}} = 1/2(1+\nu)E_{\text{eff}}$. One can estimate the first two moments of $\ln E_{\text{eff}}$ by either working directly with $F(x) = \ln E(x)$ or using the ANOVA decomposition in Eq. (2). The results are very similar. Using the ANOVA decomposition one obtains (see supplementary material: Part A)

Table 1 ANOVA fluctuation terms and their associated variances for $n = 2$ and $n = 3$

$n = 2$

Components

$\varepsilon_1(x_1) = \bar{F}_2(x_1) - \bar{F}_{12}$

$\varepsilon_2(x_2) = \bar{F}_1(x_2) - \bar{F}_{12}$

$\varepsilon_{12}(x_1, x_2) = F(x_1, x_2) - \bar{F}_{12} - \varepsilon_1(x_1) - \varepsilon_2(x_2)$

Variances

$\sigma^2_{\bar{F}_{12}} = \bar{\rho}_{12}\sigma_F^2$

$\sigma_1^2 = \text{Var}[\varepsilon_1] = (\bar{\rho}_2 - \bar{\rho}_{12})\sigma_F^2$

$\sigma_2^2 = \text{Var}[\varepsilon_2] = (\bar{\rho}_1 - \bar{\rho}_{12})\sigma_F^2$

$\sigma_{12}^2 = \text{Var}[\varepsilon_{12}] = (1 - \bar{\rho}_1 - \bar{\rho}_2 + \bar{\rho}_{12})\sigma_F^2$

$n = 3$

Components

$\varepsilon_1(x_1) = \bar{F}_{23}(x_1) - \bar{F}_{123}$

$\varepsilon_2(x_2) = \bar{F}_{13}(x_2) - \bar{F}_{123}$

$\varepsilon_3(x_3) = \bar{F}_{12}(x_3) - \bar{F}_{123}$

$\varepsilon_{12}(x_1, x_2) = \bar{F}_3(x_1, x_2) - \bar{F}_{123} - \varepsilon_1(x_1) - \varepsilon_2(x_2)$

$\varepsilon_{13}(x_1, x_3) = \bar{F}_2(x_1, x_3) - \bar{F}_{123} - \varepsilon_1(x_1) - \varepsilon_3(x_3)$

$\varepsilon_{23}(x_2, x_3) = \bar{F}_1(x_2, x_3) - \bar{F}_{123} - \varepsilon_2(x_2) - \varepsilon_3(x_3)$

$\varepsilon_{123}(x_1, x_2, x_3) = F(x_1, x_2, x_3) - \bar{F}_{123} - \varepsilon_1(x_1) - \varepsilon_2(x_2) - \varepsilon_3(x_3) - \varepsilon_{12}(x_1, x_2) - \varepsilon_{13}(x_1, x_3) - \varepsilon_{23}(x_2, x_3)$

Variances

$\sigma^2_{\bar{F}_{123}} = \bar{\rho}_{123}\sigma_F^2$

$\sigma_1^2 = (\bar{\rho}_{23} - \bar{\rho}_{123})\sigma_F^2$

$\sigma_2^2 = (\bar{\rho}_{13} - \bar{\rho}_{123})\sigma_F^2$

$\sigma_3^2 = (\bar{\rho}_{12} - \bar{\rho}_{123})\sigma_F^2$

$\sigma_{12}^2 = (\bar{\rho}_3 - \bar{\rho}_{13} - \bar{\rho}_{23} + \bar{\rho}_{123})\sigma_F^2$

$\sigma_{13}^2 = (\bar{\rho}_2 - \bar{\rho}_{12} - \bar{\rho}_{23} + \bar{\rho}_{123})\sigma_F^2$

$\sigma_{23}^2 = (\bar{\rho}_1 - \bar{\rho}_{12} - \bar{\rho}_{13} + \bar{\rho}_{123})\sigma_F^2$

$\sigma_{123}^2 = (1 - \bar{\rho}_1 - \bar{\rho}_2 - \bar{\rho}_3 + \bar{\rho}_{12} + \bar{\rho}_{13} + \bar{\rho}_{23} - \bar{\rho}_{123})\sigma_F^2$

$$\begin{aligned} m_{\ln E_{\text{eff}}} &= -\sigma_F^2 + \frac{1}{2}\ln\left[1 + \bar{\rho}_{e^F}\left(e^{\sigma_F^2} - 1\right)\right], \\ \sigma^2_{\ln E_{\text{eff}}} &= \ln\left[1 + \bar{\rho}_{e^F}\left(e^{\sigma_F^2} - 1\right)\right] \end{aligned} \tag{5}$$

and

$$\begin{aligned} m_{\ln G_{\text{eff}}} &= \ln(c) + m_{\ln E_{\text{eff}}}, \\ \sigma^2_{\ln G_{\text{eff}}} &= \sigma^2_{\ln E_{\text{eff}}} \end{aligned} \tag{6}$$

where $\bar{\rho}_{e^F}$ is the average correlation of $E = e^F$ for two points uniformly and independently located along the rod. For details on the calculation of this average correlation, see supplementary material: Part A and Part B. Notice that, except for the term $\ln(c)$ where $c = 1/2(1+\nu)$, the moments of $\ln E_{\text{eff}}$ and $\ln G_{\text{eff}}$ are identical. The spatial average $\bar{F}_1$ contributes additively to $\ln E_{\text{eff}}$ and $\ln G_{\text{eff}}$ and the fluctuation term $e^{\varepsilon_1(x)}$ contributes through its harmonic average.

It is interesting to compare the moments in Eq. (5) with those of the log average modulus $\ln(\bar{E})$. The latter is approximately normal with parameters

$$\begin{aligned} m_{\ln \bar{E}} &= -\frac{1}{2}\sigma^2_{\ln E_{\text{eff}}}, \\ \sigma^2_{\ln \bar{E}} &= \sigma^2_{\ln E_{\text{eff}}} \end{aligned} \tag{7}$$

Hence, E_{eff} has the same distribution as $[e^{-\sigma_F^2}(1 + \bar{\rho}_{e^F}(e^{\sigma_F^2} - 1))]\bar{E}$. The factor $[e^{-\sigma_F^2}(1 + \bar{\rho}_{e^F}(e^{\sigma_F^2} - 1))]$decreases from 1 to $e^{-\sigma_F^2}$ as the average correlation $\bar{\rho}_{e^F}$ decreases from 1 (constant modulus $E = e^F$ along the rod) to 0 (ergodic limit in which the average correlation of E along the rod is zero).

3.2 n = 2 ($L_1 \times L_2$ Blocks). Using the ANOVA decomposition in Eq. (3), one finds (see supplementary material: Part A.3)

$$m_{\ln E_{\text{eff},1}} = -\frac{1}{8}(5 - 5\bar{\rho}_1 + 3\bar{\rho}_2 + 5\bar{\rho}_{12})\sigma_F^2 + \frac{1}{2}\ln\left[\frac{1 + \bar{\rho}_{e^{\bar{F}_2}}\left(e^{\bar{\rho}_2\sigma_F^2} - 1\right)}{1 + \bar{\rho}_{e^{\bar{\varepsilon}_2}}\left(e^{(\bar{\rho}_1 - \bar{\rho}_{12})\sigma_F^2} - 1\right)}\right]$$

$$\sigma^2_{\ln E_{\text{eff},1}} = \ln\left[1 + \bar{\rho}_{e^{\bar{F}_2}}\left(e^{\bar{\rho}_2\sigma_F^2} - 1\right)\right] + \ln\left[1 + \bar{\rho}_{e^{\bar{\varepsilon}_2}}\left(e^{(\bar{\rho}_1 - \bar{\rho}_{12})\sigma_F^2} - 1\right)\right] \tag{8}$$

and

$$m_{\ln G_{\text{eff},12}} = \ln(c) - \frac{1}{8}\sigma_{12}^2 - \frac{1}{2}\sigma_F^2 + \frac{1}{2}\sum_{i=1}^{2}\left\{\ln\left[1 + \bar{\rho}_{e^{\varepsilon_i}}\left(e^{\sigma^2_{\varepsilon_i}} - 1\right)\right] - \sigma^2_{\varepsilon_i}\right\}$$

$$\sigma^2_{\ln G_{\text{eff},12}} = \bar{\rho}_{12}\sigma_F^2 + \sum_{i=1}^{2}\ln\left[1 + \bar{\rho}_{e^{\varepsilon_i}}\left(e^{\sigma^2_{\varepsilon_i}} - 1\right)\right] \tag{9}$$

where the various average correlations $\bar{\rho}$ are explained in supplementary material: Part A. The distribution of $\ln E_{\text{eff},2}$ is obtained by interchanging the indices 1 and 2 in Eq. (8).

Equation (8) can be understood as follows. The contribution to $\ln E_{\text{eff}_1}$ from the first two terms in Eq. (3) is obtained by reference to a 1D problem with appropriate log-modulus variance and correlation function: compare the expression $(-5/8)\sigma_F^2 + (1/2)\ln\left[1 + \bar{\rho}_{e^{\bar{F}_2}}\left(e^{\bar{\rho}_2\sigma_F^2} - 1\right)\right]$ in Eq. (8) with Eq. (5). The contribution of $\varepsilon_2(x_2)$ to $\ln E_{\text{eff}_1}$ is the arithmetic average of $e^{\varepsilon_2(x)}$, while the second-order fluctuation $\varepsilon_{12}(x_1, x_2)$ is assumed to contribute an ergodic factor to $m_{\ln E_{\text{eff}_1}}$ from Eq. (1). For the log-effective shear modulus, the effect of the spatial average $\bar{F}_{12}$ is as in Eq. (8), while the main effects $\varepsilon_1(x_1)$ and $\varepsilon_2(x_2)$ contribute through the harmonic averages of $e^{\varepsilon_1(x)}$ and $e^{\varepsilon_2(x)}$. Also in this case the second-order fluctuation effect is approximated as a deterministic ergodic factor.

The following special cases of Eq. (8) are noted:

(1) 2D ergodic case ($\bar{\rho}_1 = \bar{\rho}_2 = \bar{\rho}_{12} = 0$). Under these conditions Eq. (8) gives $\left(m_{\ln E_{\text{eff},1}} = e^{-\frac{5}{8}\sigma_F^2}, \sigma^2_{\ln E_{\text{eff},1}} = 0\right)$ in accordance with Eq. (1) for $n = 2$;
(2) 1D case $(\bar{\rho}_2 = 1, \bar{\rho}_1 = \bar{\rho}_{12} = 0) \Rightarrow \left(m_{\ln E_{\text{eff},1}} = [1 + \bar{\rho}_{e^F}\left(e^{\sigma_F^2} - 1\right)]e^{-\sigma_F^2}, \sigma^2_{\ln E_{\text{eff},1}} = \ln\left[1 + \bar{\rho}_{e^F}\left(e^{\sigma_F^2} - 1\right)\right]\right)$. This coincides with Eq. (5);
(3) 1D ergodic case $(\bar{\rho}_2 = 1, \bar{\rho}_{e^F} = \bar{\rho}_1 = \bar{\rho}_{12} = 0) \Rightarrow (m_{\ln E_{\text{eff},1}} = e^{-\sigma_F^2}, \sigma^2_{\ln E_{\text{eff},1}} = 0)$, in accordance with Eq. (1) for $n = 1$.

Case 2 above is significant as it shows that the 1D parameters in Eq. (5) are recovered in the limit $L_1/L_2 \to \infty$; hence, the 2D results are consistent with the 1D analysis. Similar special cases apply to the shear modulus in Eq. (9).

3.3 n = 3 ($L_1 \times L_2 \times L_3$ Block). Using the ANOVA decomposition in Eq. (4), the following expressions are derived in supplementary material: Part A.4:

$$m_{\ln E_{\text{eff},1}} = -\frac{1}{2}(1 - \bar{\rho}_1 + \bar{\rho}_{23} + \bar{\rho}_{123})\sigma_F^2 - \frac{1}{8}\left(\sigma_{12}^2 + \sigma_{13}^2\right) + \frac{1}{30}\sigma_{123}^2 + \frac{1}{2}\ln\left[1 + \bar{\rho}_{e^{F_{23}}}\left(e^{\bar{\rho}_{23}\sigma_F^2} - 1\right)\right] - \frac{1}{2}\ln\left[1 + \bar{\rho}_{e^{\bar{F}_1 - \bar{F}_{123}}}\left(e^{(\bar{\rho}_1 - \bar{\rho}_{123})\sigma_F^2} - 1\right)\right]$$

$$\sigma^2_{\ln E_{\text{eff},1}} = \ln\left[1 + \bar{\rho}_{e^{\bar{F}_{23}}}\left(e^{\bar{\rho}_{23}\sigma_F^2} - 1\right)\right] + \ln\left[1 + \bar{\rho}_{e^{F_1 - F_{123}}}\left(e^{(\bar{\rho}_1 - \bar{\rho}_{123})\sigma_F^2} - 1\right)\right] \tag{10}$$

$$m_{\ln G_{\text{eff},12}} = \ln(c) - \frac{1}{8}\sigma_{12}^2 + \frac{1}{15}\sigma_{123}^2 - \frac{1}{2}\sigma_F^2 + \frac{1}{2}\sum_{i=1}^{2}\left\{\ln\left[1 + \bar{\rho}_{e^{\varepsilon_i}}\left(e^{\sigma^2_{\varepsilon_i}} - 1\right)\right] - \sigma^2_{\varepsilon_i}\right\}$$

$$\sigma^2_{\ln G_{\text{eff},12}} = \bar{\rho}_{123}\sigma_F^2 + \sum_{i=1}^{2}\ln\left[1 + \bar{\rho}_{e^{\varepsilon_i}}\left(e^{\sigma^2_{\varepsilon_i}} - 1\right)\right] \tag{11}$$

where $\sigma_{12}^2, \sigma_{13}^2$, and σ_{123}^2 are given in Table 1 and the average correlations $\bar{\rho}_J$ for any given index list J are found using the distribution of R_J in supplementary material: Part B.

In analogy to the $n = 2$ case, for E_{eff_1}, we find the contribution from $\bar{F}_{123} + \varepsilon_1(x_1)$ by using the 1D results with an appropriate variance and correlation function. The remaining main effects $\varepsilon_2(x)$ and $\varepsilon_3(x)$ contribute through the arithmetic averages of $e^{\varepsilon_2(x)}$ and $e^{\varepsilon_3(x)}$, as in the 2D case. Finally, we use deterministic ergodic approximations for the effects of $\varepsilon_{12}(x_1, x_2)$, $\varepsilon_{23}(x_2, x_3)$, $\varepsilon_{13}(x_1, x_3)$, and $\varepsilon_{123}(x_1, x_2, x_3)$.

The distribution of the effective shear modulus $G_{\text{eff}_{12}}$ is found in a way similar to the $n = 2$ case. This includes the effect of the spatial average $\bar{F}_{123}$ and the effects of the two in-plane fluctuations $\varepsilon_1(x)$ and $\varepsilon_2(x)$, which contribute through the harmonic averages of $e^{\varepsilon_1(x)}$ and $e^{\varepsilon_2(x)}$. We eliminate the influence of the third main effect, $\varepsilon_3(x)$, by scaling the shear stresses by $e^{\varepsilon_3(x_3)}$ along the x_3-direction, as previously explained. The average shear strain is thus the same in each (x_1, x_2)-plane through the block. Again, we use ergodic approximations to account for $\varepsilon_{12}(x_1, x_2)$ and $\varepsilon_{123}(x_1, x_2, x_3)$, while $\varepsilon_{13}(x_1, x_3)$ and $\varepsilon_{23}(x_2, x_3)$ are assumed to have no influence on $G_{\text{eff}_{12}}$.

The remaining 3D elastic moduli are obtained by permuting the indices in Eqs. (10) and (11).

3.4 Correlation Coefficients. Expressions and derivations for the correlation coefficients for all pairs of log-moduli are presented in supplementary material: Part A. In total, there are three correlation coefficients in 2D and fifteen correlation coefficients in 3D.

The variance of the spatial average $\bar{F}_{12}$ in 2D and $\bar{F}_{123}$ in 3D is an important common contributor to the variance of all log-moduli. This is why the correlation coefficient tends to be large for all pairs of log-moduli (see Sec. 4). Pairs of log-moduli that depend on main effects in the same way (through either arithmetic or harmonic averaging) are especially highly correlated.

4 Validation and Parametric Analysis

To validate the analytical approximations, we use Monte Carlo simulation. For each simulation of the modulus field, the elastic problem is solved directly in 1D and through a finite element model in 2D and 3D, with linear four- and eight-node elements, respectively. The system is resolved on an 80×80 grid (6400 elements) in 2D and a $20 \times 20 \times 20$ grid (8000 elements) in 3D.

We simulate the Gaussian process $F(x)$ with a Karhunen-Loève expansion, with 80, 6400, and 8000 modes for the 1D, 2D, and 3D system, respectively. This is more than sufficient to accurately describe F-fields with the minimum correlation lengths used ($L_1/8$ for $n = 1$ and 2, $L_1/4$ for $n = 3$). The Karhunen–Loève expansion of the Gaussian process is a singular value decomposition of the covariance kernel [30]. All reported numerical distributions are based on 10,000 Monte Carlo simulations.

4.1 Example Validation Results. To illustrate, we present a few comparisons between numerical and analytical results involving different space dimensions n, specimen sizes, and parameters of the normal log-modulus $F = \log(E)$. For $n = 1$, we consider a bar of unit length L, correlation distance $r_0 = 0.125$, standard deviation $\sigma_F = 0.3$ and two alternative correlation functions, $\rho_F(r) = e^{-r/r_0}$ and $\rho_F(r) = e^{-(r/r_0)^2}$. In 2D, we analyze a

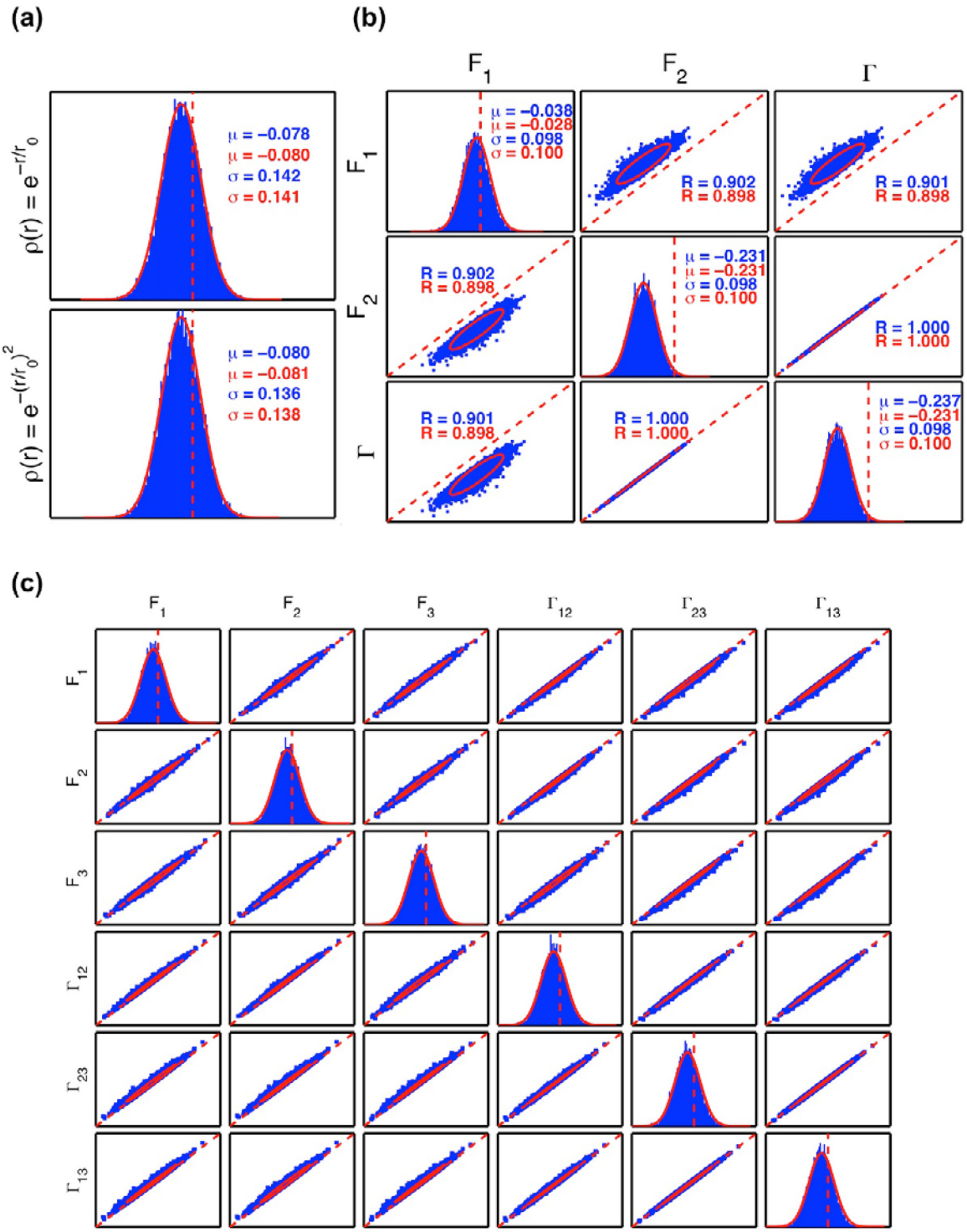

Fig. 2 (*a*) **1D rod. Comparison of theoretical (lineplots and ellipses) and numerically predicted distributions (histograms and scatter plots) of F_1 for $r_0/L = 0.125$, $\sigma_F = 0.3$ and correlation function e^{-r/r_0} or $e^{-(r/r_0)^2}$. (*b*) Comparison of theoretical and simulated distributions of the 2D elastic tensor for a rectangular block with parameters $L_2/L_1 = 100$, $r_0/L_1 = 2$, $\sigma_F = 0.5$ and correlation function e^{-r/r_0}. (*c*) Similar comparison for a cubic specimen with $r_0/L = 0.25$, $\sigma_F = 0.3$ and correlation function e^{-r/r_0}.**

rectangular specimen with side lengths $L_1 = 1$ and $L_2 = 100$, correlation length $r_0 = 2$, standard deviation $\sigma_F = 0.5$ and correlation function $\rho_F(r) = e^{-r/r_0}$. In 3D, we analyze a cubic specimen with $L = 1$, $r_0 = 0.25$, $\sigma_F = 0.3$, and correlation function $\rho_F(r) = e^{-r/r_0}$.

The results are summarized in Fig. 2 through a comparison of the marginal and bivariate distributions of the effective log-moduli $F_i = \ln E_{\text{eff}_i}$ and $\Gamma_{ij} = \ln G_{\text{eff}_{ij}}$. For $n = 1$, we show only the distribution of the effective Young's modulus since E_{eff} and G_{eff} are deterministically related. The red ellipses are theoretical 2-sigma dispersion ellipses (consider that for a sample size of 10,000, simulations from the normal distribution should be approximately enveloped by the 3-sigma dispersion ellipse). In all cases, there is good agreement between analytical approximations

and simulation results. Discrepancies, which are minor and limited to blocks with high aspect ratios, largely originate from the assumption of joint normality of the effective log-moduli: for highly elongated 2D specimens (see Fig. 2(*b*)), the transversal modulus is an upper-bound to the longitudinal modulus and this condition is inconsistent with joint normality. For $n = 3$, the correlation coefficients range between $R = 0.9941$ and $R = 0.9996$ and the difference between the analytical predictions and the numerical results is never more than 0.5% of R. Similarly good agreement between analytical and simulation results have been obtained for different block geometries and stochastic properties of the log-modulus.

As a benchmark of the efficacy of standard homogenization rules we also compute the Voigt and Reuss bounds for specimens with lognormal Young's modulus distributions. We find that for a 2D square specimen with lognormal stiffness, and exponential correlation kernel with parameters $r_0 = 0.125$ and $\sigma_F = 0.8$, the average Voigt estimate is almost a factor 2 larger than the average Reuss estimate. The discrepancy between the estimates depends on the parameters of the stochastic Young's modulus field. In future work we will present simple rules for the point estimates of effective stiffnesses based on the methodology developed here.

4.2 Parametric Analysis. Having found that the ANOVA approach produces accurate results, we use the analytical formulas to investigate how the distribution of the effective moduli varies with different controlling factors. In all cases (for $n = 1$, 2, and 3) the mean value of the log-effective moduli is bound from above by zero meaning that heterogeneity always has a softening effect (see also Fig. 2).

n = 1. Figure 3 shows the first two moments (mean m and standard deviation σ) of $\ln E_{\text{eff}}$ for 1D specimens. The moments are displayed for two different correlation functions $\rho(r)$ and a range of effective specimen lengths L/r_0, where r_0 is the correlation distance. Since the mean values are very nearly proportional to σ_F^2 and the standard deviations are very nearly proportional to σ_F, we calculate these moments under the reference condition $\sigma_F = 0.5$ and divide them by 0.25 and 0.5, respectively, to produce the standardized quantities m/σ_F^2 and σ/σ_F that are plotted in the figure. The effective shear modulus is deterministically related to the effective tensile modulus and is not shown. Interpretation of the plots is made easier by considering two extreme conditions:

(1) In the low correlation limit $L/r_0 \gg 1$, E_{eff} approaches the 1D ergodic value with $m = -\sigma_F^2$ (see Eq. (1)) and $\sigma = 0$;
(2) In the high correlation limit $L/r_0 \ll 1$, E_{eff} equals the random but nearly uniform value of E inside the rod; hence, $m = -0.5\sigma_F^2$ and $\sigma = \sigma_F$.

As the effective rod length L/r_0 varies from 0 to infinity, μ and σ vary smoothly between these two limits. The different exponents of the radii in the correlation functions lead to different decay rates of μ and σ, the Gaussian correlation function exhibits significantly faster decay.

n = 2. Figure 4 shows the first two moments (through the mean values μ, standard deviations σ, and correlation coefficients R) of the log-effective moduli $F_i = \ln E_{\text{eff},i}$ and $\Gamma = \ln G_{\text{eff}}$ for 2D blocks. The plots cover a wide range of aspect ratios L_2/L_1 and normalized correlation lengths r_0/L_1. As for $n = 1$, we calculate the mean values and standard deviations for $\sigma_F = 0.5$ and normalize them by 0.5 and 0.25 to obtain the normalized moments plotted in the figure. The correlation coefficients do not display a simple dependence on σ_F, but to avoid cluttering we show them only for $\sigma_F = 0.5$ (in other work, not presented here, we have calculated R for different values of σ_F and observed similar trends).

To understand Fig. 4, it is useful to think of three reference regimes: the longitudinal regime when the specimen is highly elongated in the stretching direction (hence, when $L_2/L_1 \ll 1$ for F_1 and $L_2/L_1 \gg 1$ for F_2), the square-like regime $L_2/L_1 \approx 1$, and the transversal regime when the specimen is much thinner in the stretching direction. We denote by $L_{\min} = \min\{L_1, L_2\}$ and $L_{\max} = \max\{L_1, L_2\}$ the minimum and maximum side lengths of the specimen; hence, when $L_{\min} \ll r_0 \ll L_{\max}$, the 2D specimen behaves like a 1D rod. Properties of the effective moduli under limiting conditions involving the above regimes are:

(1) When $L_{\min} \ll r_0 \ll L_{\max}$, the modulus E varies longitudinally along the rod but not transversally. The effective longitudinal modulus equals the harmonic average of E with $m/\sigma_F^2 = -1$, whereas the effective transversal modulus equals the arithmetic average of E with $m/\sigma_F^2 = 0$;
(2) Irrespective of the aspect ratio L_2/L_1, in the low correlation limit $r_0 \ll L_{\min}$, E_{eff_1}, and E_{eff_2} approach the 2D ergodic value with $m/\sigma_F^2 = -5/8$;
(3) When $r_0 \gg L_{\max}$, E_{eff_1}, and E_{eff_2} equal the random but nearly uniform value of E inside the specimen. Therefore, $m/\sigma_F^2 = -0.5$ for both moduli.

In cases 1 and 2, the effective moduli are deterministic (therefore $\sigma/\sigma_F = 0$), whereas in case 3 the effective moduli are maximally uncertain with $\sigma/\sigma_F = 1$. Many of the plots in Fig. 4 display transitions between two or more of the above limiting cases (of course the limiting cases themselves are never exactly realized due to finite range of the parameter values considered). Next we point at some such transitions and at general features of the results.

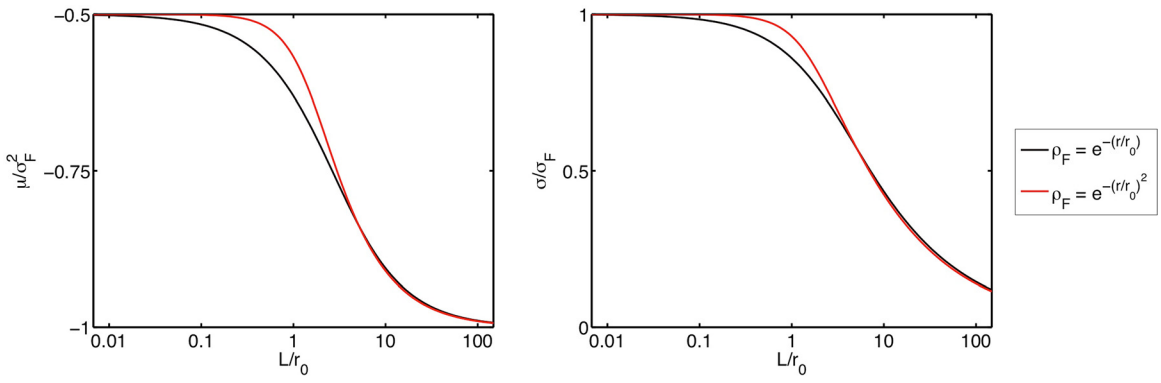

Fig. 3 Normalized mean and standard deviation of the effective Young's modulus of a 1D rod as a function of the dimensionless specimen length L/r_0, for correlation functions $e^{-(r/r_0)}$ and $e^{-(r/r_0)^2}$. As $L/r_0 \to \infty$ the mean value tends to the deterministic ergodic limit, while the standard deviation tends to 0.

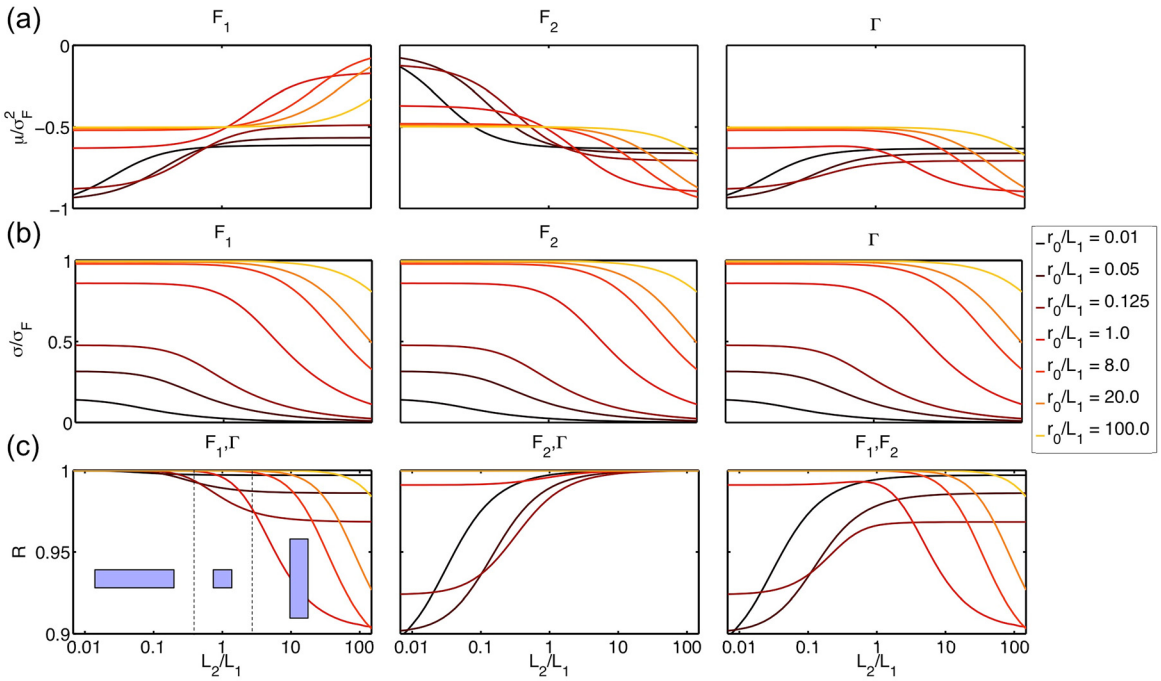

Fig. 4 Parameters of the effective elastic tensor of a 2D rectangular block as a function of the aspect ratio L_2/L_1 and the normalized correlation distance r_0/L_1. The correlation function is e^{-r/r_0}. The correlation coefficients are shown for $\sigma_F = 0.5$. The longitudinal, square-like, and transversal regimes are indicated in the low left panel.

m_{F_1}. First consider the mean value of the effective log-modulus F_1 in the case of low correlation ($r_0/L_1 = 0.01$, black curve). As L_2/L_1 increases, one observes a transition from the first (longitudinal) to the second (ergodic) limiting condition. By the time the specimen is square, the transition is essentially complete and m_{F_1} remains nearly constant in the transversal regime. At the other correlation extreme (highest correlation with $r_0/L_1 = 100$, yellow curve), all modulus fluctuations are negligible for longitudinal and square-like specimens. Hence, in these cases, the third limiting condition is met and $m_{F_1}/\sigma_F^2 = -0.5$. As the ratio L_2/L_1 becomes very large, the transversal limit is approached and the first limiting condition is met. The behavior of m_{F_1} in other correlation cases can be understood by considering that values of m/σ_F^2 close to 0, -0.5, $-5/8$, and -1 are, respectively, associated with arithmetic averaging, no averaging, ergodic conditions, and harmonic averaging of the modulus field.

m_{F_2}. The plots of m_{F_2} are similar but inverted relative to those of m_{F_1}. The transitions between different regimes occur at the same aspect ratios L_2/L_1, but since stretching is now in the x_2 direction, the longitudinal and transversal regimes are interchanged.

m_Γ. Apart from the factor $c = 1/2(1+\nu)$, the main difference between the effective shear and longitudinal moduli is that the main-effect fluctuations of F have a harmonic exponentiated-averaging effect in shear and a harmonic or arithmetic exponentiated-averaging effect in tension. Under ergodic conditions, these main effects are negligible and the $-5/8$ rule applies to all moduli, in shear and tension. In combination, these considerations lead to the approximate rule $m_\Gamma = \ln(c) + \min\{m_{F_1}, m_{F_2}\}$.

σ. The normalized standard deviations in Fig. 4(*b*) are identical for all three log-moduli. The reason is that the variance of the log arithmetic average of a lognormal field is very nearly the same as the variance of its log harmonic average. In general, for a given correlation length r_0, σ decreases as the specimen size increases. This is why, for any given dimensionless correlation distance r_0/L_1, σ decreases as the aspect ratio L_2/L_1 increases. The highest values of σ, close to σ_F, are found when the log-modulus F has near-perfect correlation inside the specimen.

Correlations. Figure 4(*c*) shows the correlation coefficients R for the three pairs of log-moduli. A general observation is that in all cases R is above 0.9. The highest values, close to 1, are obtained in the ergodic and high-spatial-correlation regimes. The lowest values are between moduli that depend significantly on the first-order fluctuations of the log-modulus, but are obtained through different averaging operations (arithmetic or harmonic) of E. Examples for F_1 and F_2 are cases with low correlation and small L_2/L_1 or high correlation and large L_2/L_1. Relatively low correlations are also seen between F_1 or F_2 and Γ when one of the F moduli is close to the arithmetic average of E (stretching in the transversal direction).

$n = 3$. Figure 5 uses a format similar to Fig. 4 to show results for a 3D rectangular block with $L_1 = L_2 = L = 1$ and different normalized correlation lengths r_0/L and box heights L_3/L. Since we have set $L_1 = L_2$, the log Young's moduli F_1 and F_2 and the log shear moduli Γ_{13} and Γ_{23} have identical distributions. As for $n = 1$ and $n = 2$, we calculate all parameters for $\sigma_F = 0.5$ and divide the mean values and standard deviations by 0.5 and 0.25, respectively. Also like for $n = 2$, the correlation coefficients are shown for $\sigma_F = 0.5$. Of the eight unique correlation coefficients (R_{F_1,F_2}, R_{F_1,F_3}, $R_{F_1,\Gamma_{12}}$, $R_{F_1,\Gamma_{13}}$, $R_{F_3,\Gamma_{12}}$, $R_{F_3,\Gamma_{13}}$, $R_{\Gamma_{12},\Gamma_{13}}$, $R_{\Gamma_{13},\Gamma_{23}}$), we display three representative ones ($R_{F_1,\Gamma_{13}}$, $R_{F_3,\Gamma_{13}}$, R_{F_1,F_3}).

Results are qualitatively similar to those for $n = 2$. In particular, one may notice transitions between various regimes: the thin-plate regime when $L_3/L \ll 1$, the cube-like regime when $L_3/L \approx 1$, and the elongated regime when $L_3/L \gg 1$. The quantitative differences from the 2D case are mainly explained by the fact that, as $L_3/L \to 0$, the block in Fig. 5 becomes a thin square plate, whereas under $L_2/L_1 \to 0$ the block in Fig. 4 becomes a thin 1D rod. A closer analogy can be drawn (and much closer results are observed) between the log-moduli F_2 in Fig. 4 and F_3 in Fig. 5.

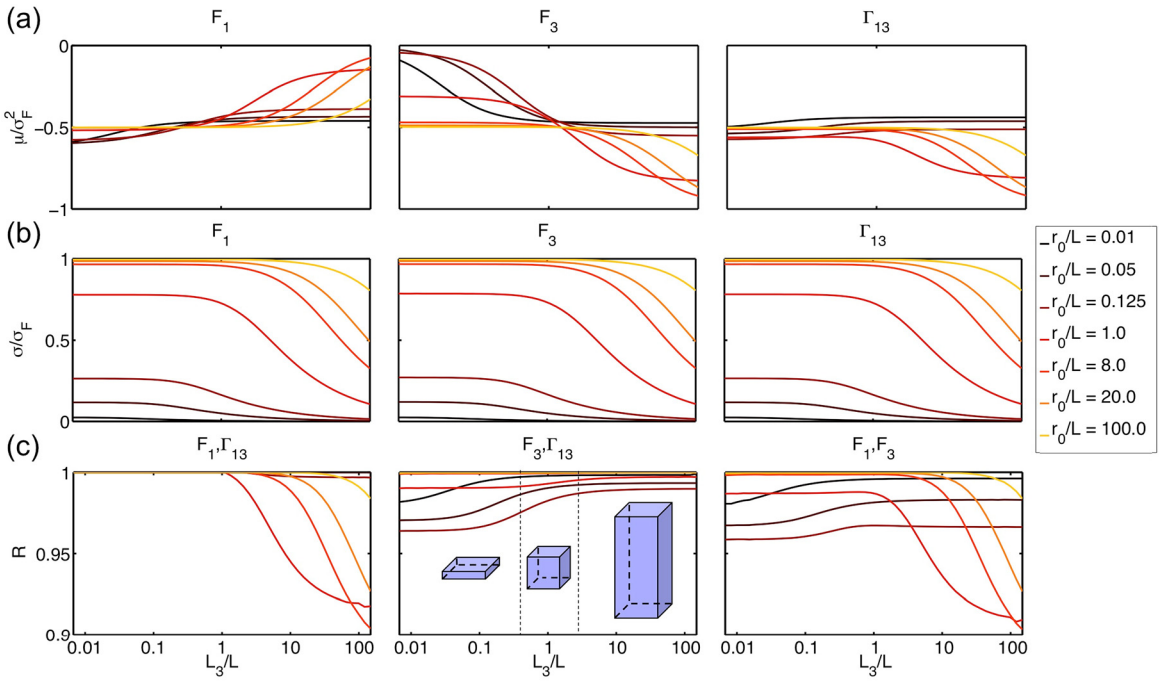

Fig. 5 Parameters of the effective elastic tensor for a 3D rectangular block with side lengths $L_1 = L_2 = L$ and L_3, as a function of the aspect ratio L_3/L and the normalized correlation distance r_0/L_1. The correlation function is e^{-r/r_0}. The correlation coefficients are for $\sigma_F = 0.5$. The plate-like, cube-like, and elongated regimes are indicated in the center low panel.

5 Conclusions

We have studied the effective elastic moduli of 1D, 2D, and 3D rectangular blocks when the log Young's modulus $F(x) = \ln E(x)$ varies spatially as a normal random field. By using an ANOVA decomposition that expresses $F(x)$ as a constant plus a number of first- and higher-order fluctuation terms and analyzing each ANOVA term in turn, we developed analytical (joint lognormal) approximations to the distribution of the effective elastic tensor. To our knowledge, this is the first time that this problem has been addressed analytically. The advantage of an analytical approach over simulation is that the results are either in closed form or computable at relatively low cost, making it possible to use them for parametric analysis and ultimately for reliability-based design and optimization.

Due to various simplifying assumptions, the results are approximate, but we have found very good correspondence with Monte Carlo simulations for a wide range of geometric and stochastic parameters. The accuracy of the first two moment predictions (mean values, variances and correlation coefficients of the log-moduli) is high. The main differences come from the fact that the assumption of joint lognormal distribution is not always verified: for certain geometric configurations and loading conditions, one modulus may be known to be larger than another, whereas under joint lognormality constraints of this type cannot be imposed.

We used the analytical results to explore the dependence of the distribution of the log-effective elasticity tensor on various geometric parameters (Euclidean dimension $n = 1$, 2, or 3, specimen size, aspect ratios) and probabilistic characteristics (log-modulus variance, correlation distance, shape of the correlation function). We identified limiting conditions under which it is easy to understand the main features of the distribution of the log-effective elasticity tensor and highlighted transition regimes between these limiting conditions.

In all cases we observed a softening in the mean effective log-moduli induced by the heterogeneity. Moreover, simple approximate rules were obtained and verified through simulation. One such rule is that the log-variances of all tensor components can be taken to be the same. Another is that in most cases the log-moduli are very strongly correlated; hence, in first-order approximation one could assume perfect dependence, reducing the computational task to evaluating only the mean values and common variance of the log-moduli. Exceptions to this second rule involve moduli that depend significantly on different averages (typically arithmetic for one, harmonic for the other) of the exponentiated first-order fluctuations of $F(x)$.

Future extensions of this work include the following:

(1) Application of the moments of the effective moduli as parameters of building blocks in larger scale structural systems;
(2) Application of the ANOVA approach and the lognormal approximation to other classes of randomly heterogeneous materials, in particular, materials with different types of random multiphase inclusions and possibly random within-phase variation of the elastic modulus;
(3) Development of simple rules to approximate the effective elasticity tensor given a spatial pattern of Young's modulus $E(x)$. While much work has been done on this problem in the past, we are interested in seeing whether homogenization rules based on the ANOVA/lognormal approach can outperform existing rules.
(4) Application of the ANOVA approach to other effective properties, such as the effective strength and fracture toughness of randomly heterogeneous specimens.

The general aim of these extensions is to develop analytical tools to characterize and control the mechanical effects of random material heterogeneities, and make it possible to design materials with superior reliability properties.

Acknowledgment

We acknowledge support from BASF-NORA, NSF, and PECASE.

References

[1] Beran, M. J., 1968, "Monographs in Statistical Physics and Thermodynamics," *Statistical Continuum Theories*, Vol. xv, Interscience Publishers, New York, p. 424.

[2] Kachanov, M., and Sevostianov, I., 2013, *Effective Properties of Heterogeneous Materials*, Vol. 193, Springer, Dordrecht, The Netherlands.

[3] Nemat-Nasser, S., and Hori, M., 1993, *Micromechanics: Overall Properties of Heterogeneous Materials*, Vol. xx (North-Holland Series in Applied Mathematics and Mechanics), North-Holland, Amsterdam, The Netherlands, p. 687.

[4] Sanchez-Palencia, E., Zaoui, A., and International Centre for Mechanical Sciences, 1987, "Homogenization Techniques for Composite Media: Lectures Delivered at the CISM International Center for Mechanical Sciences," (Lecture Notes in Physics, Udine, Italy, July 1–5, 1985, Vol. ix), Springer-Verlag, Berlin, Germany, p. 397.

[5] Torquato, S., 2002, *Random Heterogeneous Materials: Microstructure and Macroscopic Properties*, Vol. 16, Springer, New York.

[6] Gupta, H. S., Stachewicz, U., Wagermaier, W., Roschger, P., Wagner, H. D., and Fratzl, P., 2006, "Mechanical Modulation at the Lamellar Level in Osteonal Bone," J. Mater. Res., **21**(8), pp. 1913–1921.

[7] Tai, K., Dao, M., Suresh, S., Palazoglu, A., and Ortiz, C., 2007, "Nanoscale Heterogeneity Promotes Energy Dissipation in Bone," Nature Mater., **6**(6), pp. 454–462.

[8] Younis, S., Kauffmann, Y., Blouch, L., and Zolotoyabko, E., 2012, "Inhomogeneity of Nacre Lamellae on the Nanometer Length Scale," Cryst. Growth Des., **12**(9), pp. 4574–4579.

[9] Zhang, T., Li, X., Kadkhodaei, S., and Gao, H., 2012, "Flaw Insensitive Fracture in Nanocrystalline Graphene," Nano Lett., **12**(9), pp. 4605–4610.

[10] Dimas, L. S., Giesa, T., and Buehler, M. J., 2014, "Coupled Continuum and Discrete Analysis of Random Heterogeneous Materials: Elasticity and Fracture," J. Mech. Phys. Solids, **63**, pp. 481–490.

[11] Veneziano, D., 2003, *Computational Fluid and Solid Mechanics*, Elsevier, Cambridge, MA.

[12] Ostoja-Starzewski, M., 1998, "Random Field Models of Heterogeneous Materials," Int. J. Solids Struct., **35**(19), pp. 2429–2455.

[13] Ghanem, R., and Spanos, P. D., 1990, "Polynomial Chaos in Stochastic Finite-Elements," ASME J. Appl. Mech., **57**(1), pp. 197–202.

[14] Stefanou, G., 2009, "The Stochastic Finite Element Method: Past, Present and Future," Comput. Methods Appl. Mech. Eng., **198**(9–12), pp. 1031–1051.

[15] Vanmarcke, E., and Grigoriu, M., 1983, "Stochastic Finite-Element Analysis of Simple Beams," ASCE J. Eng. Mech., **109**(5), pp. 1203–1214.

[16] Ngah, M. F., and Young, A., 2007, "Application of the Spectral Stochastic Finite Element Method for Performance Prediction of Composite Structures," Compos. Struct., **78**(3), pp. 447–456.

[17] Pellissetti, M. F., and Ghanem, R. G., 2000, "Iterative Solution of Systems of Linear Equations Arising in the Context of Stochastic Finite Elements," Adv. Eng. Software, **31**(8–9), pp. 607–616.

[18] Yamazaki, F., Shinozuka, M., and Dasgupta, G., 1988, "Neumann Expansion for Stochastic Finite-Element Analysis," ASCE J. Eng. Mech., **114**(8), pp. 1335–1354.

[19] Huyse, L., and Maes, M. A., 2001, "Random Field Modeling of Elastic Properties Using Homogenization," ASCE J. Eng. Mech., **127**(1), pp. 27–36.

[20] Ostojastarzewski, M., and Wang, C., 1989, "Linear Elasticity of Planar Delaunay Networks—Random Field Characterization of Effective Moduli," Acta Mech., **80**(1–2), pp. 61–80.

[21] Arwade, S. R., and Deodatis, G., 2011, "Variability Response Functions for Effective Material Properties," Probab. Eng. Mech., **26**(2), pp. 174–181.

[22] Graham-Brady, L., 2010, "Statistical Characterization of Meso-Scale Uniaxial Compressive Strength in Brittle Materials With Randomly Occurring Flaws," Int. J. Solids Struct., **47**(18–19), pp. 2398–2413.

[23] Ma, J. A., Temizer, I., and Wriggers, P., 2011, "Random Homogenization Analysis in Linear Elasticity Based on Analytical Bounds and Estimates," Int. J. Solids Struct., **48**(2), pp. 280–291.

[24] Shinozuka, M., and Deodatis, G., 1988, "Response Variability of Stochastic Finite-Element Systems," ASCE J. Eng. Mech., **114**(3), pp. 499–519.

[25] Shinozuka, M., 1987, "Structural Response Variability," ASCE J. Eng. Mech., **113**(6), pp. 825–842.

[26] Teferra, K., Arwade, S. R., and Deodatis, G., 2012, "Stochastic Variability of Effective Properties Via the Generalized Variability Response Function," Comput. Struct., **110**, pp. 107–115.

[27] Teferra, K., Arwade, S. R., and Deodatis, G., 2014, "Generalized Variability Response Functions for Two-Dimensional Elasticity Problems," Comput. Methods Appl. Mech. Eng., **272**, pp. 121–137.

[28] Veneziano, D., and Tabaei, A., 2001, "Analysis of Variance Method for the Equivalent Conductivity of Rectangular Blocks," Water Resour. Res., **37**(12), pp. 2919–2927.

[29] See supplemental material at for detailed derivations of the equations and supplementary results.

[30] Karhunen, K., 1946, *Zur Spektraltheorie Stochastischer Prozesse*, Ann. Acad. Sci. Fenn., Ser. A, 37.